Journal of Colloid and Interface Science 567 (2020) 243–255

Contents lists available at ScienceDirect

Journal of Colloid and Interface Science

journal homepage: www.elsevier.com/locate/jcis

Hummers' and Brodie's graphene oxides as photocatalysts for phenol degradation

Marta Pedrosa [a], Eliana S. Da Silva [a], Luisa M. Pastrana-Martínez [b], Goran Drazic [c], Polycarpos Falaras [d], Joaquim L. Faria [a], José L. Figueiredo [a], Adrián M.T. Silva [a,*]

[a] Laboratory of Separation and Reaction Engineering – Laboratory of Catalysis and Materials (LSRE-LCM), Faculdade de Engenharia, Universidade do Porto, Rua Dr. Roberto Frias, 4200-465 Porto, Portugal
[b] Carbon Materials Research Group, Department of Inorganic Chemistry, Faculty of Sciences, University of Granada, Campus Fuentenueva s/n, 18071 Granada, Spain
[c] Department for Materials Chemistry, National Institute of Chemistry, Hajdrihova 19, SI-1000 Ljubljana, Slovenia
[d] National Centre for Scientific Research "Demokritos", Institute of Nanoscience and Nanotechnology, 15341, Agia Paraskevi Attikis, Athens, Greece

HIGHLIGHTS

- Hummers' (GO-H) and Brodie's (GO-B) GO materials were tested in photocatalysis.
- GO-B promoted high phenol degradation under near UV/Vis and visible irradiation.
- GO-H and GO-B had different surface chemistries, d-distance and photoluminescence.
- Holes and hydroxyl radicals were the main reactive species in play.
- GO-B is active under visible illumination and stable in reusing cycles.

GRAPHICAL ABSTRACT

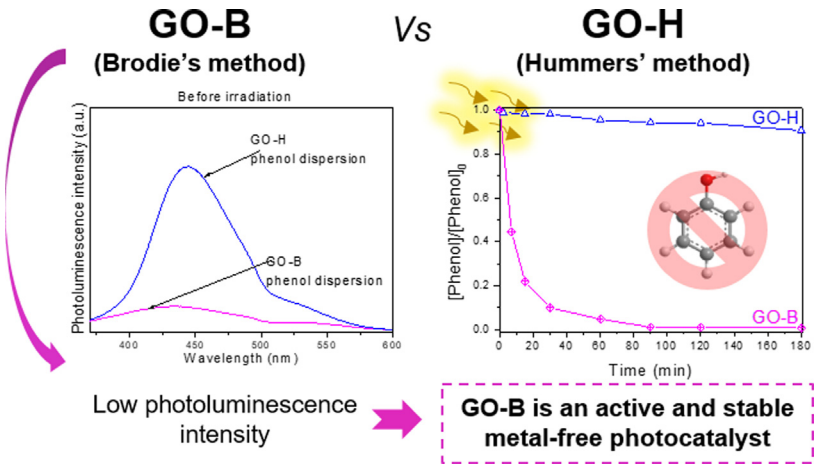

ARTICLE INFO

Article history:
Received 14 October 2019
Revised 22 January 2020
Accepted 24 January 2020
Available online 27 January 2020

Keywords:
Photocatalysis
Graphene oxide
Metal-free
Surface chemistry
Photoluminescence

ABSTRACT

Undoped metal-free graphene oxide (GO) materials prepared by either a modified Hummers' (GO-H) or a Brodie's (GO-B) method were tested as photocatalysts in aqueous solution for the oxidative conversion of phenol. In the dark, the adsorptive capacity of GO-B towards phenol (~35%) was higher than that of GO-H (~15%). Upon near-UV/Vis irradiation, GO-H was able to remove 21% of phenol after 180 min, mostly through adsorption. On the other hand, by using less energetic visible irradiation, GO-B removed as much as 95% in just 90 min. By thorough characterization of the prepared materials (SEM, HRTEM, TGA, TPD, Raman, XRD, XPS and photoluminescence) the observed performances could be explained in terms of their different surface chemistries. The GO-B presents the lower concentration of oxygen functional groups (in particular carbonyl groups as revealed by XPS) and it has a considerably higher photocatalytic activity compared to GO-H. Photoluminescence (PL) of liquid dispersions and XRD analysis of powders showed lower PL intensity and smaller interlayer distance for GO-B relative to GO-H, respectively: this suggests lower electron-hole recombination and enhanced electron transfer in GO-B, in support of its boosted photocatalytic activity. Reusability tests showed no efficiency loss after a second usage cycle and over three runs under visible irradiation, which was in line with the similarity of the XPS spectra

* Corresponding author.
E-mail address: adrian@fe.up.pt (A.M.T. Silva).

https://doi.org/10.1016/j.jcis.2020.01.093
0021-9797/

of the fresh and used GO-B materials. Moreover, scavenging studies revealed that holes and hydroxyl radicals were the main reactive species in play during the photocatalytic process. The obtained results, establish for the first time, that GO prepared by Brodie's method is an active and stable undoped metal-free photocatalyst for phenol degradation in aqueous solutions, opening new paths for the application of more sustainable and metal-free materials for water treatment solutions.

1. Introduction

Graphene and its derivatives have been employed to produce photocatalysts with applications in different fields, such as environmental remediation and energy conversion [1–20]. Graphite has been used as a source of graphene analogues. A top-down approach can be used to produce graphene derivatives, by graphite oxidation and subsequent exfoliation to graphene oxide (GO), or direct liquid exfoliation of graphite with macromolecules or organic solvents [21,22]. GO is composed of carbon atoms arranged in a hexagonal lattice and decorated with oxygen functional groups on the basal plane defects (epoxy and hydroxyl groups, C—O) and at the edges (carboxyl groups, O=C—O) of the layer [11,23]. The occurrence of carbonyl groups (C=O, as quinones or ketones) in the basal plane of GO derivatives, mainly on the edges of structural defects, has also been described [24]. In 2010, Erickson and coworkers reported hydroxyl and epoxies, as the main oxygenated groups in GO, and the presence of carbonyl groups at the edges of holes (<5 nm^2) in the GO structure [25]. This carbon material presents sp^2-hybridized carbon domains (conducting π-states) separated by a large energy gap from the sp^3-linked carbons (σ-states) covalently bonded to oxygen groups [11,26]. The alteration of the sp^2 and sp^3 portions of GO (e.g., by oxidation or reduction) can tune its properties, including the band-gap energy as well as other features such as insulating, semiconducting or semi-metallic properties [11,26]. The introduction of oxygen atoms into the graphene layer disrupts the carbon lattice, increasing the band-gap energy proportionally to the oxygen abundance, since graphene is a zero-band-gap material [11]. For instance, reduced GO (rGO) is a conducting material with a shorter band-gap than GO. The reduction process may contribute both to the formation of nanopores in the location of the lost oxygenated groups of GO and the production of CO or CO_2 from the loss of carbon atoms from the basal plane under UV irradiation [26,27]. Partial reduction of GO has also been observed upon long periods of continuous illumination, as carbon photogenerated electrons may target oxygenated groups of GO instead of the organic pollutant molecule [11]. During this process, GO can be photochemically transformed not only into rGO and CO_2 but also into persistent by-products such as polycyclic aromatic carbons (PAHs) [28].

Most of the research published so far using GO in photocatalysis for the degradation of organic contaminants involves its combination with metals [6–12,16–18,29] or doping with non-metals [13–15]. In fact, undoped metal-free GO materials are still uncommon in photocatalysis for the degradation of organic pollutants [30–35]. In addition, these GO materials are either commercial or prepared the by Hummers' method, while the particular application of Brodie's-based GO materials for the photocatalytic degradation of organic contaminants has not been reported in the literature, as far as we know. For instance, Adeleye *et al.* [30] reported 11% of bisphenol A degradation after 24 h of solar light irradiation using a commercially available GO material. Li *et al.* [32] obtained almost complete removal of hydroquinone in 30 min, under white light emitting diode (LED) irradiation employing another commercial GO powder. Oh *et al.* [31] prepared GO by Hummers' method, resulting in 19% of rhodamine B degradation after 2 h under visible light irradiation. Bustos-Ramirez *et al.* used GO derived from Hummers' method to remove 38% of phenol [33] and 97% of 4-chlorophenol [34] with an UV lamp (254 nm) in ~2 h. Peréz-Ramirez and co-workers [35] reported 73% of dye (Reactive Red 2) degradation, under UV irradiation (254 nm) in 1 h, using GO derived from the Hummers' method. However, only ca. 5% of increment was ascribed to the photocatalytic activity in comparison with adsorption, meaning that the GO material was an active adsorbent of the studied anionic dye.

Hence, it is now of paramount importance to investigate undoped GO photocatalysts prepared by different methodologies including Brodie's method, which can provide materials with different characteristics [36–42] and, as a consequence, various photocatalytic activities are expected. To the best of our knowledge, we are reporting for the first time the comparison of undoped metal-free GO materials prepared by Hummers' and Brodie's methodologies for the photocatalytic degradation of phenol as a well-recognized probe molecule, considering the surface chemistry, interlayer distance and photoluminescence in the liquid dispersions.

2. Experimental

2.1. Chemicals

All solutions were prepared with ultrapure water. Phenol ($C_6H_6O \geq 99\%$), sodium azide ($NaN_3 \geq 99.5\%$), ethylenediaminetetraacetic acid (EDTA ≥ 99%) and barium sulfate ($BaSO_4$, > 98%) were purchased from Sigma-Aldrich. Methanol (CH_3OH, HPLC grade ≥ 99.8%), sodium hydroxide (NaOH, ≥ 98.5%) and 2-propanol (C_3H_8O, HPLC grade) were obtained from VWR, hydroquinone ($C_6H_6O_2$, ≥ 99.5%) from Merck and *p*-benzoquinone ($C_6H_4O_2$, 99%) from Acrōs Organics. TiO_2 Aeroxide® P25 (80% anatase: 20% rutile) powder was obtained from Evonik (hereafter referred to as P25 TiO_2). Sodium chloride (NaCl, > 99%) was purchase from José Manuel Gomes dos Santos and hydrochloric acid (HCl, 37%) from VWR Chemicals.

2.2. Production of graphene oxide by Hummers' and Brodie's methods

Graphite oxide was synthesized by Brodie's - B [37,43] and Hummers' - H [37,44] methods, as reported elsewhere [8]. The obtained oxidized materials were dispersed in deionized water and exfoliated using an ultrasonic processor (UP400S, 24 kHz) for 1 h [8,16]. The GO dispersions were evaporated at 60 °C, resulting in GO-H (Hummers'-based GO) and GO-B (Brodie's-based GO) samples.

2.3. Characterization techniques

Thermogravimetric analysis (TGA) was performed with a STA490 PC/4/H Luxx Netzsch thermal analyser. The sample was heated from 50 to 500 °C, at 5 °C min^{-1} in a nitrogen atmosphere.

Temperature programmed desorption (TPD) analysis was performed in a fully automated AMI-300 Catalyst Characterization

Instrument (Altamira Instruments) with a quadrupole mass spectrometer (Dymaxion, Ametek). The sample (~25 mg) was placed in a U-shaped quartz tube and heated at 5 °C min^{-1} up to 1060 °C under a constant flow rate of helium (25 cm^3 min^{-1}).

X-ray photoelectron spectroscopy (XPS) analysis was conducted with a Kratos AXIS Ultra HSA apparatus, equipped with a monochromatic Al Kα X-ray source, operating at 15 kV (90 W) in Fixed Analyser Transmission (FAT) mode with a pass energy of 40 eV for regions of interest (C1s and O1s) and 80 eV for survey. Data acquisition was achieved with a charge neutralization system and a pressure lower than 10^{-6} Pa. To reduce the sample charging effect the binding energies were calibrated by referencing the C1s peak at 285 eV and an analysis area of 300 μm × 700 μm were used. CasaXPS software was employed to analyze and deconvolute the obtained spectra.

Raman spectra were collected with a Renishaw inVia Reflex spectrometer equipped with two excitation sources, i.e. an Ar^+ ion laser (λ = 514.5 nm) and a high power near infrared (NIR) diode laser (λ = 785 nm). To focus the laser beam, a 20 × short distance magnification lens was used, which provided a power energy of 0.04 mW μm^{-2}. Frequency shifts were calibrated by an internal Si reference. Several spectra were collected from different spots for each sample.

A PANalytical X'Pert MPD apparatus equipped with a X'Celerator detector and secondary monochromator (Cu Kα λ = 0.154 nm, 40 kV, 30 mA; the data was recorded at a 0.017° step size, 100 s/step) was used for the X-ray diffraction (XRD) analysis.

Scanning electron microscopy (SEM) was performed to evaluate the morphology of GO, using a Quanta 400 FEG ESEM / EDAX Genesis X4M electron microscope.

A Cs probe-corrected TEM/STEM Jeol ARM 200 CF equipment with a cold-FEG electron source, operated at 80 kV was used for high-resolution transmission electron microscopy (HR-TEM) and scanning transmission electron microscopy (STEM) analysis. A Gatan Quantum ER double electron energy loss spectroscopy (EELS) system and a Jeol Centurio 100 mm^2 energy dispersive X-ray spectrometer (EDXS) were used for elemental analyses and mapping in STEM. Ethanol was used to disperse the samples before their placement on a copper lacy-carbon coated grid.

A JASCO V-560 UV/Vis spectrophotometer, with an integrating sphere attachment (JASCO ISV-469), was employed to study the near-UV/Vis diffuse reflectance (DRS UV–Vis) of GO materials ($BaSO_4$ was used as reference).

Steady-state photoluminescence (PL) spectra were recorded with a JASCO FP-8300 spectrofluorometer equipped with a 150 W Xe lamp. The PL spectra of GO powders and of the aerated aqueous dispersions containing phenol and GO before and after irradiation (filtered to retain the GO) were obtained under excitation at 320 nm, using emission and excitation bandwidths of 10 nm. The absorbance of the aqueous dispersions was ca. 0.1–0.2 at the excitation wavelength in order to avoid inner effects. The fluorescence emission spectrum was thus obtained by subtracting the spectrum of the sample to the solvent (water) spectrum in order to remove the contribution of the solvent Raman peak.

N_2 adsorption-desorption isotherms were obtained at −196 °C in a Quantachrome NOVA 4200e apparatus. Prior to the analysis, all samples were outgassed for 3 h at 120 °C.

The determination of the point of zero charge (pH_{PZC}) was based on previous studies [45,46]. Briefly, 5 mL of 0.01 mol L^{-1} NaCl was placed in a flask and the pH was adjusted to a value between 2 and 12 by adding 0.1 mol L^{-1} HCl or 0.1 mol L^{-1} NaOH. Then, 0.015 g of sample was added and the final pH was measured after 24 h under stirring at room temperature. The pH_{PZC} is the point where the curve pH_{final} versus $pH_{initial}$ crosses the line $pH_{initial} = pH_{final}$.

2.4. Photocatalytic experiments

The experiments were conducted in a cylindrical glass reactor equipped with a Heraeus TQ 150 medium-pressure mercury vapor lamp located axially in the reactor and held in a quartz immersion tube. A DURAN 50® glass cooling jacket was used for irradiation in the near-UV/Vis (λ > 365 nm) and water refrigeration at 25 °C. Visible illumination (λ > 400 nm) was produced using sodium nitrite as a UV cut-off liquid filter under recirculation with cooling to keep the same temperature of 25 °C. The irradiance of the lamp (330 and 285 W m^{-2} for near-UV/Vis and visible, respectively) was measured using a calibrated Modular USB series spectrometer from Ocean Optics. A phenol solution (5.0 mg L^{-1} with a pH adjusted to ~7.0 with NaOH) was prepared and used to disperse GO materials (1.0 g L^{-1} with pH of 2.8 or 4.9 with GO-H and GO-B, respectively). 150 mL of this dispersion was irradiated under constant stirring after a dark adsorption-desorption equilibrium period of 60 min. Experiments in the absence of GO (photolysis) were also conducted. Additional experiments with scavengers of reactive oxygen species (ROS) were performed under visible illumination by adding 0.05 mol L^{-1} of EDTA, NaN_3 or 2-propanol to 5.0 mg L^{-1} of phenol, and then adjusting the pH to the neutral value. Samples were filtered (OlimPeak PTFE 0.45 μm, Teknokroma) prior to analysis.

2.5. Analytical techniques

The phenol concentration was monitored by high-performance liquid chromatography (HPLC) using a Hitachi Elite Lachrom apparatus equipped with an L-2450 diode array detector (λ = 271 nm) and a Lichrocart Purospher® Star RP-18 endcapped column (250 mm × 4.6 mm, 5 μm particles, from Merck), at room temperature. The mobile phase (70% water and 30% methanol) was employed in a gradient step at a flow rate of 1 mL min^{-1} and an injection volume of 50 μL. The phenol reaction intermediates, i.e. *p*-benzoquinone (λ = 246 nm) and hydroquinone (λ = 290 nm) were identified in the same chromatographic runs by comparison with reference standards.

3. Results and discussion

3.1. Characterization of GO materials

Several techniques were used to characterize GO-H and GO-B. The TGA results (Fig. 1) reveal ca. 45 and 25 wt% loss for GO-H

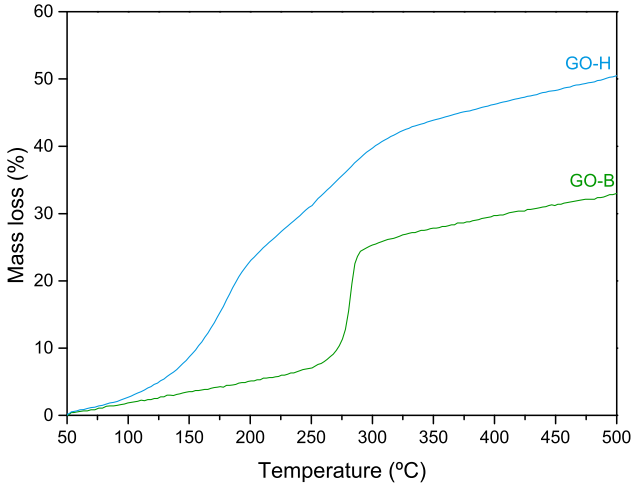

Fig. 1. TGA analysis of the carbon materials, GO-H and GO-B, under nitrogen atmosphere.

and GO-B up to 300 °C, in line with the literature [40], indicating that GO-H has a higher oxygen content [37].

TPD analysis of the GO-H sample revealed peaks at 176 and 193 °C in both CO_2 (Fig. 2a) and CO profiles (Fig. 2b), which are attributed to epoxy (known as unstable groups decomposing at lower temperatures, ca. 160–180 °C) and hydroxyl groups (190–200 °C), respectively [47]. Carboxylic anhydrides are also present at 400–550 °C although being less evident than the former ones. The additional peak observed in the CO_2 profile at 254 °C corresponds to carboxylic acids, whereas the evolution of groups as CO at higher temperatures corresponds to phenols (nearly 650 °C) and carbonyl/quinones (identified at 906 °C). Regarding GO-B, there is a sharp peak at 266 °C in both CO and CO_2 profiles, which cannot be attributed to carboxylic acids since these functionalities evolve as CO_2 only. Moreover, epoxy and hydroxyl groups were not released at the predicted temperatures (below 200 °C). Thus, this sharp increase is likely due to a sudden loss of epoxy and hydroxyl groups, confined between the tight layers of GO-B (i.e. smaller interlayer distance than GO-H, as described below), and as a consequence suffering additional exfoliation and reduction. This conclusion is supported by TGA analysis since the sharp loss of volatiles in GO-B (Fig. 1) takes place at the same temperature observed for the sharp peak in TPD (Fig. 2a and b). Thus, in the case of GO-B, epoxy and hydroxyl groups seem to evolve together with some possible carboxylic groups. GO-B also presents phenol and carbonyl/quinone groups, as demonstrated by the CO profile at the higher temperatures.

The XPS analysis provided further elucidation on the oxygenated functional groups of both materials (Fig. 3a–d). A higher overall percentage of oxygen in GO-H (34.60 at.%) in comparison with GO-B (25.80 at.%) was observed, in line with the TGA analysis. The higher oxygen content in GO-H was expected, as oxidations using permanganate (as in Hummers' method) tend to create an elevated percentage of oxygen in these carbon materials, in particular carbonyl and carboxyl groups, whereas those using chlorate (as in the case of Brodie's method) typically introduce less and more uniformly distributed oxygen functionalities [42,48]. The XPS spectra of the C1s region for GO-H (Fig. 3a) and GO-B (Fig. 3b) showed four peaks at binding energies of: (i) 285.00; (ii) 286.89–287.20; (iii) 288.62–288.97; and (iv) 290.41–290.48 eV, corresponding to (i) C═C, C—H or C—C; (ii) epoxy and hydroxyl (C—O) groups; (iii) carbonyl (C═O); and (iv) carboxyl (O═C—O) groups, respectively [3,16,37,49]. A higher percentage of C═O is found in GO-H (8.65 at.% at 288.97 eV) comparatively to GO-B (1.29 at.% at 288.62 eV), while the percentage of C—O groups in GO-B (53.83 at.% at 286.89 eV) is higher than in GO-H (46.96 at.% at 287.20 eV). The O-functionalities in GO-B (Fig. 3d) and GO-H (Fig. 3c) obtained from the deconvolution of O1s region are distributed as C—O from epoxy and hydroxyl groups (87.57 at.% at 532.54 eV and 74.00 at.% at 532.89 eV, respectively), C═O from carbonyl or quinones (2.30 at.% at 530.75 eV and 17.01 at.% at 531.78 eV, respectively) and –OH (10.13 at.% at 533.30 eV and 8.99 at.% at 533.92 eV, respectively) [3,49,50]. The considerably higher percentage of C—O groups in both materials was expected since epoxy and hydroxyl groups located on the basal planes' defects are the major oxygen functionalities in GO materials, whereas carbonyl and carboxyl groups are less representative [16,25]. Moreover, it is interesting to note the higher percentage of C═O in GO-H comparatively to GO-B, as given by the deconvolution of the C1s and the O1s regions of both materials and suggesting fewer carbonyl groups in GO-B (Fig. 2b).

We have previously reported the FTIR-ATR spectra of both materials with relation to the photocatalytic degradation of diphenhydramine using TiO_2–based composites [8]. These results corroborate the data obtained by TGA and XPS analysis in the present work. Both GO derivatives (GO-H and GO-B) present the characteristic FTIR absorption bands of C—O (epoxy, ether or peroxide groups) and C—OH [16]. GO-H exhibits an additional band (1720 cm^{-1}) that is not evident in GO-B, corresponding to the C═O stretch of carbonyl groups and/or O—C═O stretching vibration of carboxyl groups [40,41,51]. That, together with broader band in GO-H at ca. 3300 cm^{-1} may suggest a higher degree of oxidation in this material. Besides, nitrogen adsorption isotherms (Figure S1) of GO-H and GO-B reveal low nitrogen uptakes, as well as low BET surface areas (±5 $m^2\ g^{-1}$, within the equipment detection limit [8]) in accordance with other studies for this type of materials [52–55]. The low BET surface areas of GO-H and GO-B in the dried powder could be due to the tight stacking of GO layers [48]. Consequently, different behaviors have been observed for dried GO powders and hydrated materials, namely concerning the *d*-distance [40,56] and often their adsorptive capacity [57]. Oxygenated functionalities of GO derivatives, specifically epoxy groups, have been reported as relevant surface adsorption sites for SO_2 [58] and/or NH_3 [53,54,57–59] gaseous molecules. In the present work, the amount of epoxy groups in GO-B is higher than in GO-H, as revealed by XPS analysis (Fig. 3), which may potentiate the adsorptive capacity of GO-B, as demonstrated below.

The points of zero charge (pH_{PZC}) of GO-B and GO-H (Figure S2) were between ca. 2–3. These values are in good agreement with values reported in the literature for GO materials [16,60], revealing their highly acidic nature.

The Raman spectra of the two graphene derivatives are shown in Fig. 4a. In GO-H, the D and G bands appeared at 1351 and 1607 cm^{-1}, respectively, whereas they D and G band shifted to

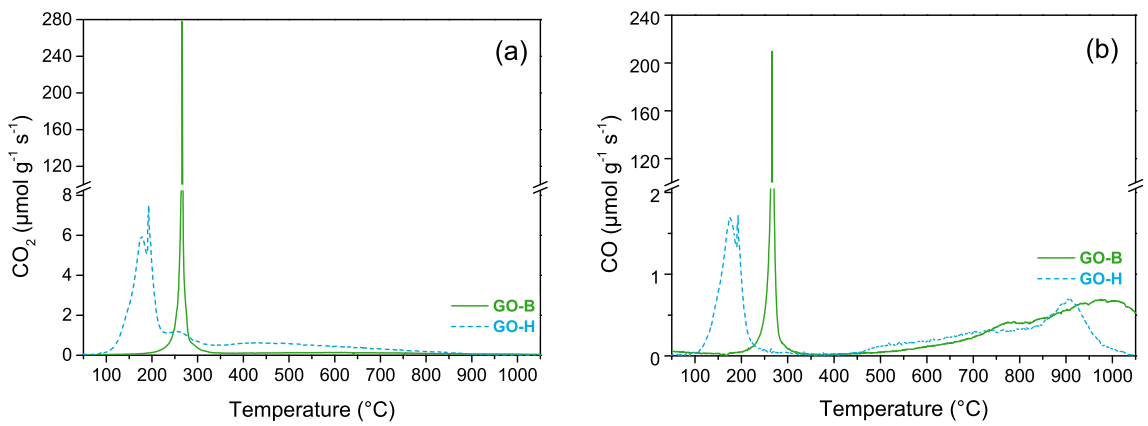

Fig. 2. TPD profiles for GO-H and GO-B: (a) CO_2 and (b) CO release.

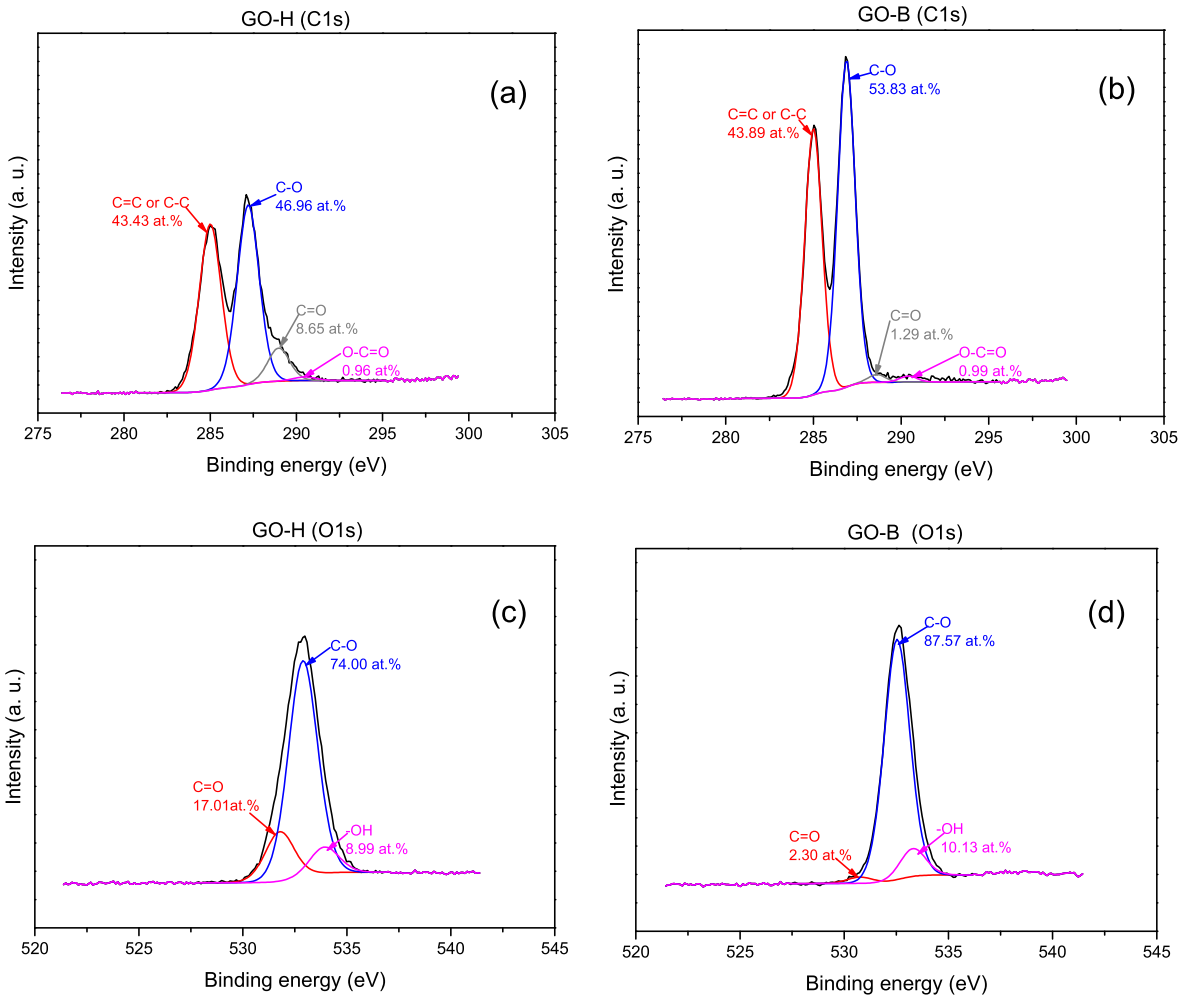

Fig. 3. XPS spectra for the deconvoluted C1s and O1s regions of GO-H (a and c, respectively) and GO-B (b and d, respectively).

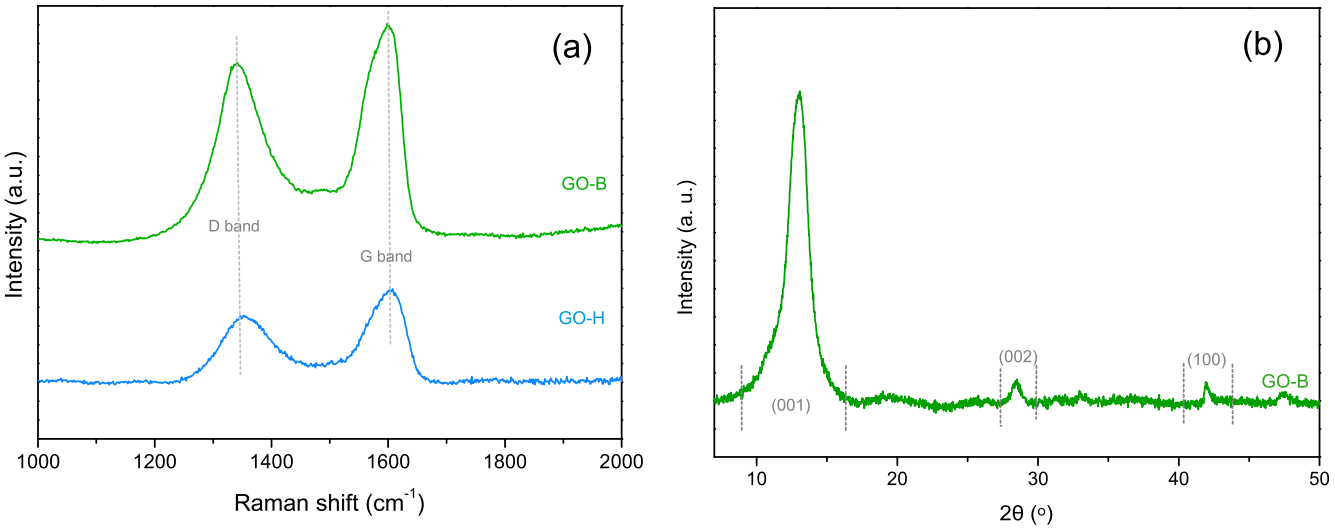

Fig. 4. Raman spectra of GO-H and GO-B excited at 514.5 nm (a) and XRD pattern of the GO-B carbon material (b).

1342 and 1598 cm^{-1} for GO-B. The intensity ratio (I_D/I_G) obtained from the integrated areas of the corresponding bands can be related to the frequency of defects in the carbon honeycomb [10]. The I_D/I_G ratios were 1.04 and 1.08 for GO-H and GO-B, respectively, which may indicate a slightly more defective structure of GO-B. Similar I_D/I_G ratios have been previously reported by Botas and co-workers for Hummers' and Brodie's based graphite oxides [37]. GO-B was also characterized by XRD in the present work (Fig. 4b), while the corresponding analysis for GO-H is reported in our previous work focused on persulfate activation [61]. For GO-H and GO-B, the (0 0 1) diffraction peak was observed at 2θ = 11.95° and 13.06°, respectively. The interlayer distance

(*d*-distance) calculated by Braggs' law applied to the (0 0 1) diffraction peak is 0.74 and 0.68 nm, respectively. A smaller *d*-distance in the materials obtained by Brodie's method in opposition to those derived from Hummers' method has been already reported [37,40]. Also, the presence of more O-functional groups in GO-based materials can be related to the larger spacing between layers [62], which is in agreement with the present results. Moreover, GO-H and GO-B presented a (1 0 0) diffraction peak at around 42.5° indicating a short-range order in stacked graphene layers [61,63,64], whereas GO-B presents a clear small (0 0 2) diffraction peak at $2\theta = 28.51°$ more likely to appear due to some unoxidized graphite [24].

The morphology of the carbon materials was evaluated by SEM (Fig. 5), both presenting the typical sheet-like appearance.

HRTEM was used to characterize GO-B, which was the best performing material as discussed below, including high-angle annular dark-field (HAADF-STEM) mode and EELS spectra (Fig. 6). The aggregated flakes (Fig. 6a and b) under magnification in atomically resolved HAADF-STEM micrographs (Fig. 6c and d) display bright spots indicative of oxygen atoms, as previously reported for GO-H [61]. Moreover, both GO-B and GO-H displayed π^* and σ^* peaks in the carbon K-edge EELS spectra, which can be associated to the sp^2 carbon hybridization [65], whereas an evident peak in the oxygen K-edge spectra was observed for GO-H only [61], in agreement with its higher degree of oxidation.

3.2. Photocatalytic activity

The photocatalytic performance of the synthesized carbon materials was studied towards the degradation of phenol (Ph), an organic pollutant commonly used as a reference compound. Photocatalytic experiments were initially carried out under near-UV/Vis irradiation (UV/Vis, irradiance of 330 W m^{-2}) (Fig. 7a). An initial 60 min of dark phenol adsorption on both carbon materials revealed that GO-H adsorbed ~15% of phenol, whereas with GO-B the adsorption increased up to ~35%, and it was kept stable from the moment of contact to the final 60 min. Since the surface areas of GO-H and GO-B are very low, the adsorption mechanism of GO-B seems to be governed by the establishment of hydrogen bonds and π-π stacking interactions [32,66,67]. Moreover, electrostatic attractions between the protonated phenol molecules and the negative surface charge of the GO-B photocatalyst were more likely favored than those with the neutral surface charge of GO-H, suggesting that the adsorptive behavior of this reaction system is pH dependent [66,67].

Once near-UV/Vis irradiation was turned-on, the phenol removals were higher than 99% in the presence of GO-B after 90 min of irradiation, whereas the value dropped to 21% in the presence of GO-H at 180 min (i.e., mostly attributed to the adsorption capacity of the material). The different photocatalytic performances of GO-H and GO-B reflect the distinct properties associated with the GO derivatives, namely their oxygen-rich functional groups, interlayer distance, phenol adsorptive capacity and energy transition upon light absorption as discussed below. As shown by XPS (Fig. 3), both materials revealed different trends in the distribution of oxygenated functionalities, in which a higher percentage of carbonyl groups was observed in GO-H (8.65 at.%) relatively to GO-B (1.29 at.%). Furthermore, the XRD pattern of GO-B (Fig. 4) revealed its smaller interlayer distance in comparison to GO-H [61], which most likely facilitated the electronic transfer in GO-B, thus resulting in a higher photocatalytic activity for this material. Moreover, as aforementioned, more phenol was adsorbed

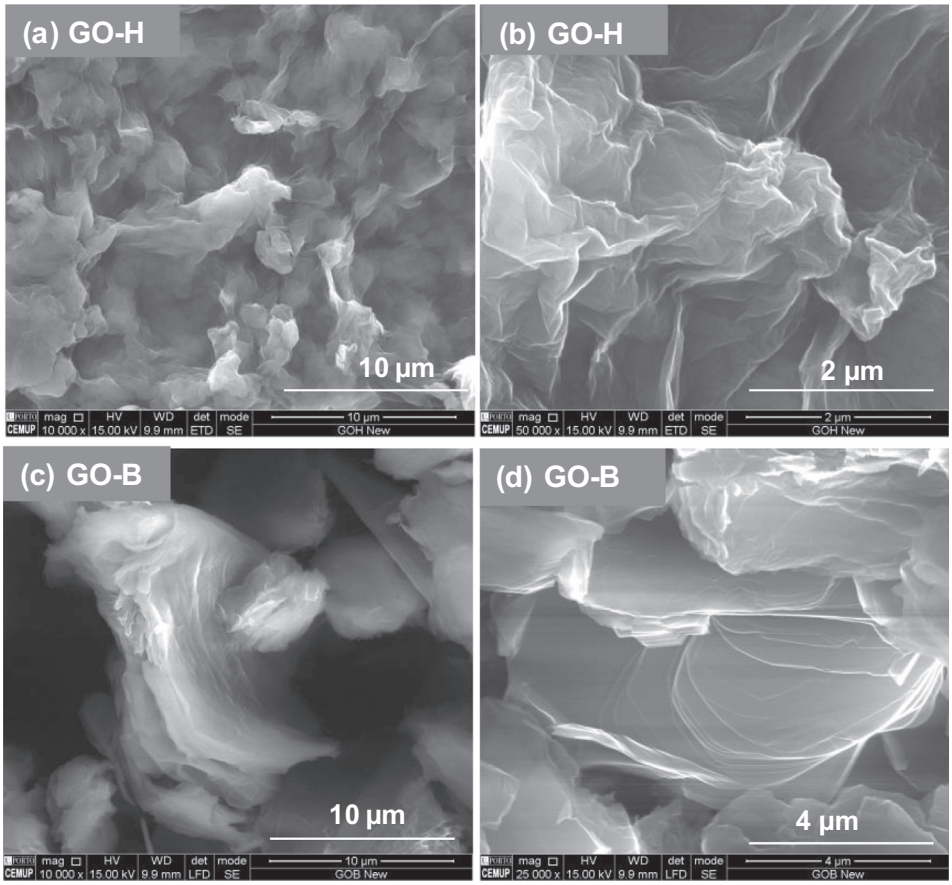

Fig. 5. SEM micrographs of (a, b) GO-H and (c, d) GO-B.

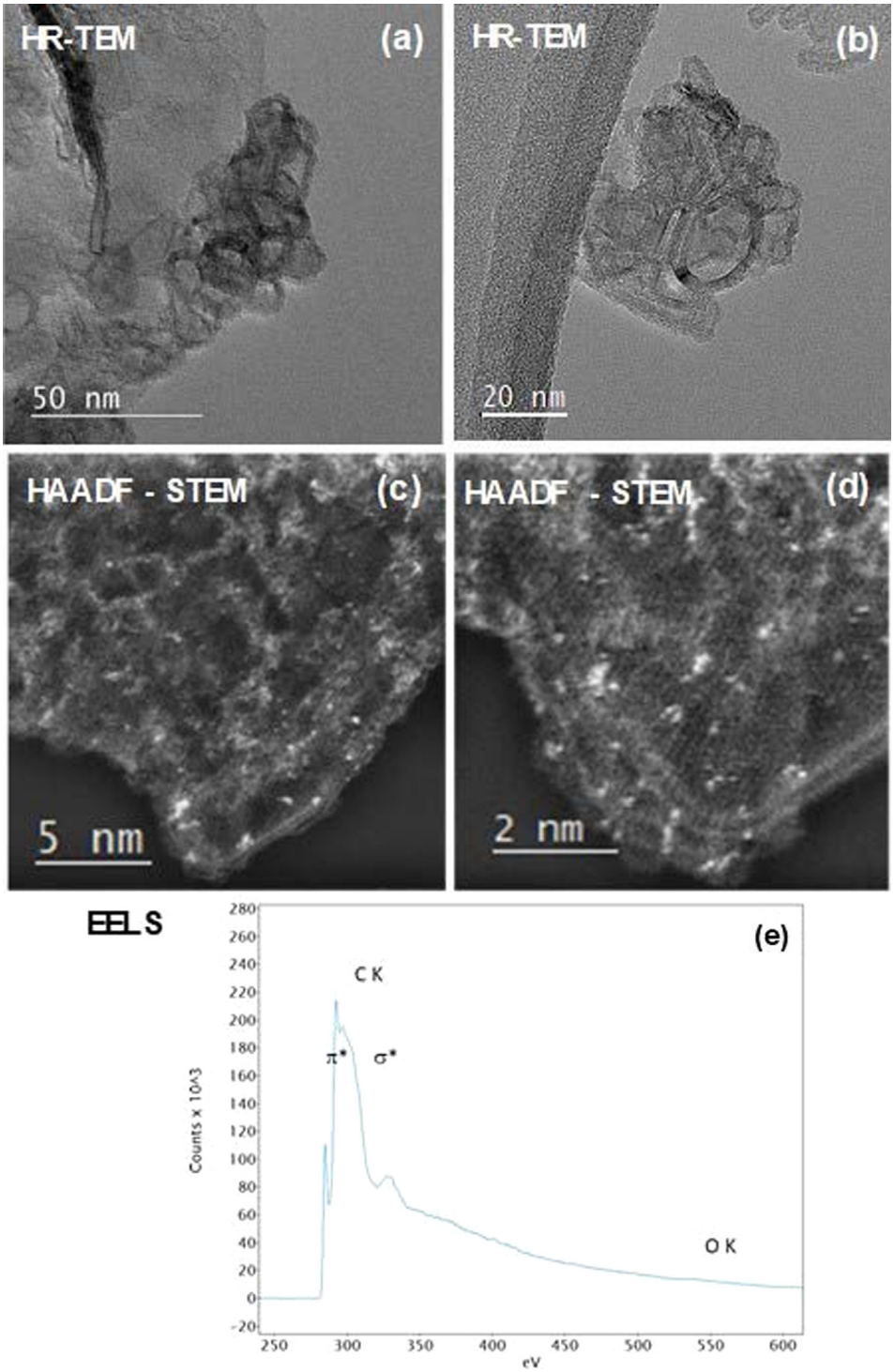

Fig. 6. Electron microscopy analysis of GO-B: (a,b) HRTEM micrographs; (c,d) HAADF-STEM; and (e) EELS spectrum.

in GO-B than in GO-H under dark conditions (Fig. 7a), suggesting a better contact between the GO material and phenol molecules in the case of GO-B, probably due to the establishment of hydrogen bonds and π-π stacking [32], promoting electronic transfer. Moreover, before irradiation, the photoluminescence (PL) intensity of GO-B phenol dispersion was lower than that of GO-H phenol dispersion (Fig. 8c). This indicates a lower electron-hole recombination in the case of GO-B, thus being in line with its enhanced photocatalytic performance.

Next, and given the recent trends and advantages concerning the use of visible light, the near-UV/Vis radiation (λ > 365 nm) was replaced by visible light (λ > 400 nm) to investigate the effect of the best performing photocatalyst (GO-B) in phenol degradation. Under these conditions, 95% of phenol was eliminated at 90 min. Its removal was higher than 97% at 180 min (Fig. 7b), even when decreasing the catalyst load to 0.5 mg L^{-1}. The activity of the carbon materials was compared with the widely studied P25 TiO_2 photocatalyst for the degradation of 5.0 mg L^{-1} of phenol under visible illumination, the results revealing a slower phenol degradation using P25 TiO_2 as photocatalyst, due to its limited absorption in the visible range of the spectrum. Furthermore, a similar behavior with GO-H and GO-B was observed for the photocatalytic

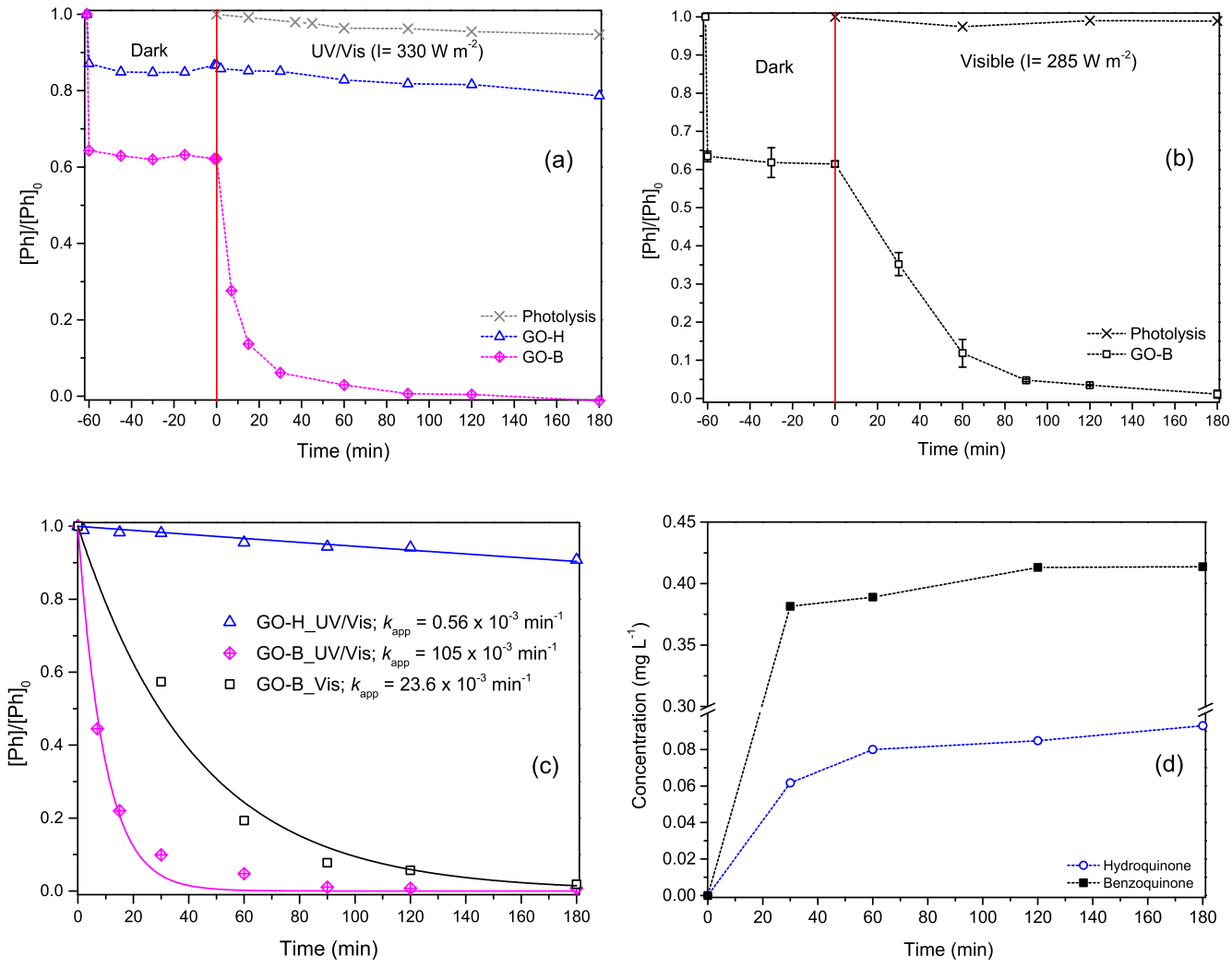

Fig. 7. Normalized phenol (Ph) concentration (a) in the dark and under near-UV/Vis (UV/Vis) irradiation using 1.0 g L^{-1} of both GO-H and GO-B, (b) in the dark and under visible (Vis) illumination using GO-B, and (c) respective pseudo-first order reaction rate constants, k_{app}. (d) Concentration of reaction by-products, *p*-benzoquinone and hydroquinone, under Vis illumination using GO-B.

degradation of phenol either with or without adjusting the initial phenol concentration to similar values after adsorption and prior to illumination (Figure S3). As shown in Fig. 7c, slower reaction kinetics are observed under visible illumination (pseudo-first order reaction rate constant, k_{app} = 23.6 × 10^{-3} min^{-1}) comparatively to near-UV/Vis (k_{app} = 105 × 10^{-3} min^{-1}), which may be primarily attributed to the lower irradiance of the light source (285 W m^{-2}) and to the lower absorption intensity of GO-B above 400 nm (Fig. 8a). As expected, the photolysis of phenol does not take place under these conditions (Fig. 7b) since it does not absorb light in the visible region. The prime reaction photoproducts, *p*-benzoquinone and hydroquinone, were quantified (Fig. 7d). The concentration of both by-products increased with the irradiation time, the *p*-benzoquinone increase being higher. The carbon concentration due to phenol is 3.63 mg L^{-1} at the beginning of the experiment, while after 180 min under visible illumination the carbon concentration due to hydroquinone and *p*-benzoquinone corresponds to ~9% of the initial carbon content. The same by-products were identified throughout the photocatalytic degradation of phenol with GO-B under near-UV/Vis irradiation and, as expected, these compounds were not detected under dark conditions. All these results indicate that phenol degradation with GO-B is due to a photocatalytic process.

In order to obtain information on the separation efficiency of the photogenerated electrons and holes and on the surface defects in GO, photoluminescence spectroscopy was employed [68–70]. The PL spectra for the most active photocatalyst (GO-B) were obtained in solid state and in the form of aqueous dispersion upon excitation at 320 nm (Fig. 8b). Both spectra depict a broad PL emission with two main emission zones, one with maximum emission below 500 nm and another above 500 nm with maximum centred at 535 nm. Two emission bands with peak maxima at ca. 440 and 500–600 nm corresponding to the blue band and the long wavelength (LW) band have been reported for GO dispersions [71]. The position of the band centred at 535 nm does not seem to change with the medium (solid state or aqueous dispersion) whereas the first band presents two maxima values (ca. 465 and 485 nm) in solid state, shifting to a single maximum at 435 nm in aqueous dispersion (Fig. 8b). This emission band (around 465–485 nm) is ascribed to the recombination of electron-hole pairs due to the presence of oxygenated groups in GO-B, whereas the presence of surface defects accounts for the emission at 535 nm [72]. The PL of the filtered solutions of phenol and GO-B (GO-B_Initial) or GO-H (GO-H_Initial) before and after irradiation (GO-B_UV/Vis, GO-B_Vis, GO-H_UV/Vis) is shown in Fig. 8c. GO-H_Initial has a red shift to higher wavelengths with a maximum

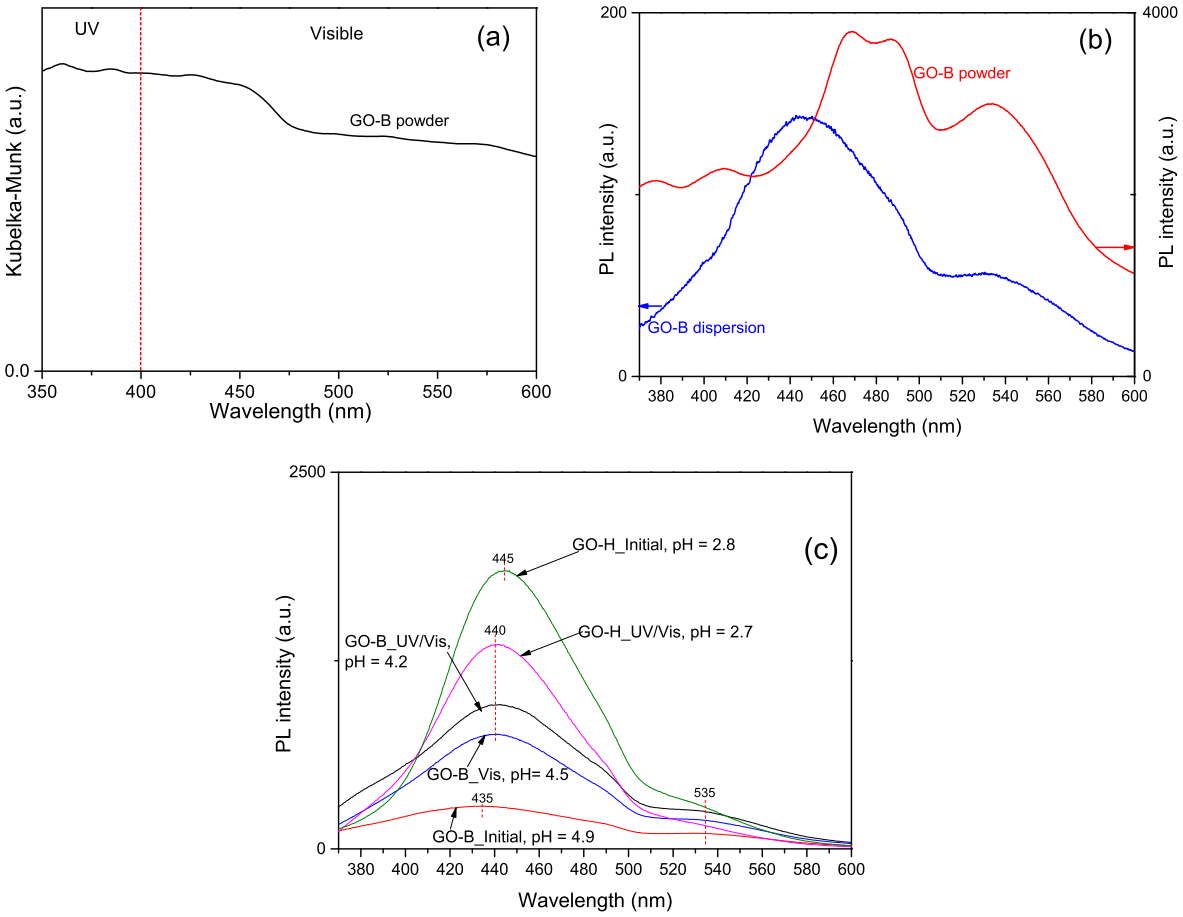

Fig. 8. (a) DRS (UV–Vis) and (b) PL spectra of GO-B in solid state and aqueous dispersion (excitation wavelength at 320 nm). (c) PL spectra of the filtered phenol solution before (initial) and after irradiation (near-UV/vis: UV/vis or visible: Vis irradiation) with GO-B (excitation at 320 nm).

of 445 nm comparatively to GO-B_Initial that has a maximum at 435 nm and a considerably lower PL intensity. The lower PL of GO-B-Initial compared to GO-H_Initial suggests lower electron-hole recombination, and thus higher photocatalytic activity for GO-B, which matches the photocatalytic results presented in Fig. 7a.

Additionally, the pH of the initial solutions was different, for GO-H_Initial and GO-B_Initial being 2.8 and 4.9, respectively. After irradiation with near-UV/Vis, the trend observed between the two carbon materials was again distinct, with the PL intensity of the irradiated GO-B (GO-B_UV/Vis) being higher than for GO-B_Initial, the opposite occurring in the case of GO-H, as irradiated GO-H_UV/Vis had less PL intensity than GO-H_Initial. These differences might be due to the formation of phenol fluorescent by-products [73], which can contribute to increase the PL intensity in the case of GO-B. In fact, the visual inspection of the color of the solutions after 180 min is in agreement with this suggestion as the solution with GO-B had a more distinct brown transparent color than that with GO-H, suggesting higher yield of photoproducts in the presence of GO-B.

On the other hand, the GO-B solution irradiated in the visible range (GO-B_Vis) presented an even lower PL intensity compared to near-UV/Vis (GO-B_UV/Vis), although both exhibited the same maximum of emission at 440 nm. Once again, this decrease of PL might be due to the lesser irradiance of the lamp in the visible range, possibly decreasing the amount of phenol fluorescent by-products. Besides, the pH values in the beginning and after irradiation with GO-H were very similar (2.8 and 2.7, respectively), whereas with GO-B (pH of GO-B_Initial was 4.9) a more substantial pH decrease was observed after illumination with both near-UV/Vis (GO-B_UV/Vis, pH of 4.2) and visible (GO-B_Vis, pH of 4.5) light. This more pronounced pH change with GO-B suggests a more efficient degradation of phenol with the formation of photoproducts, as corroborated by the photocatalytic results, ending up with the possible opening of the aromatic ring and formation of low molecular weight carboxylic acids, as reported in the literature [74]. An attempt to identify acidic photo-products (i.e. lactic, formic or acetic acids) was made in the present work. However, these intermediate species were below the detection limit, given that the initial phenol concentration was also low (5.0 mg L^{-1}) for this type of analysis.

3.3. Reactive species involved in the GO-B photocatalytic degradation of phenol

The involvement of reactive oxygen species (ROS) such as singlet oxygen, hydroxyl radicals and the superoxide anion on pollutant degradation is well documented for other systems [30,32]. Several trapping experiments were carried out under visible illumination to assess the participation of ROS. We used 2-propanol, NaN_3 and EDTA as scavengers for hydroxyl radicals, singlet oxygen and holes, respectively (Fig. 9). As shown in Fig. 9, the presence of EDTA remarkably slowed down the photocatalytic degradation of phenol. The effect is much less pronounced by adding 2-propanol, and negligible with NaN_3. After 180 min of visible irradiation, 68 and 91% of phenol was removed in the presence of EDTA and 2-propanol, respectively, compared with more than 97% of removal in the absence of these scavengers. These results suggest

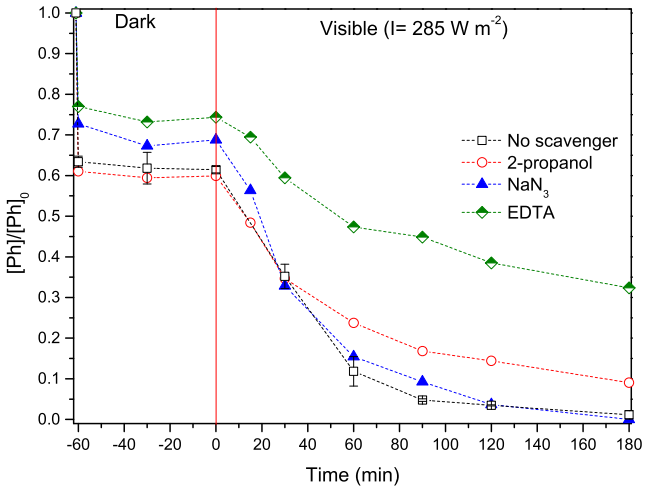

Fig. 9. Scavenger studies of phenol (Ph) using EDTA, NaN_3 or 2-propanol with GO-B under visible illumination.

that the holes formed in the valence band of GO-B and the hydroxyl radicals play a significant role in phenol degradation. Although benzoquinone is usually used as trapping agent for superoxide anion radicals [75–77], the potential effect of this radical was not tested in the current work since this phenolic compound is also a reaction by-product of the photocatalytic degradation of phenol.

3.4. Photocatalyst stability

An essential feature for the application of a photocatalytic process is the stability of the catalyst. Therefore, reusability of the best performing carbon material (GO-B) was assessed under visible illumination by withdrawing samples from the reactor every 60 min (Fig. 10a), rather than 30 min, to recover more material at the end of each run. We used GO-B for three cycles of phenol removal without losses in its photocatalytic activity from the 2nd to the 3rd run (92 and 91% of phenol removal at 180 min, respectively), the 1st run being influenced by more significant phenol adsorption during the dark period.

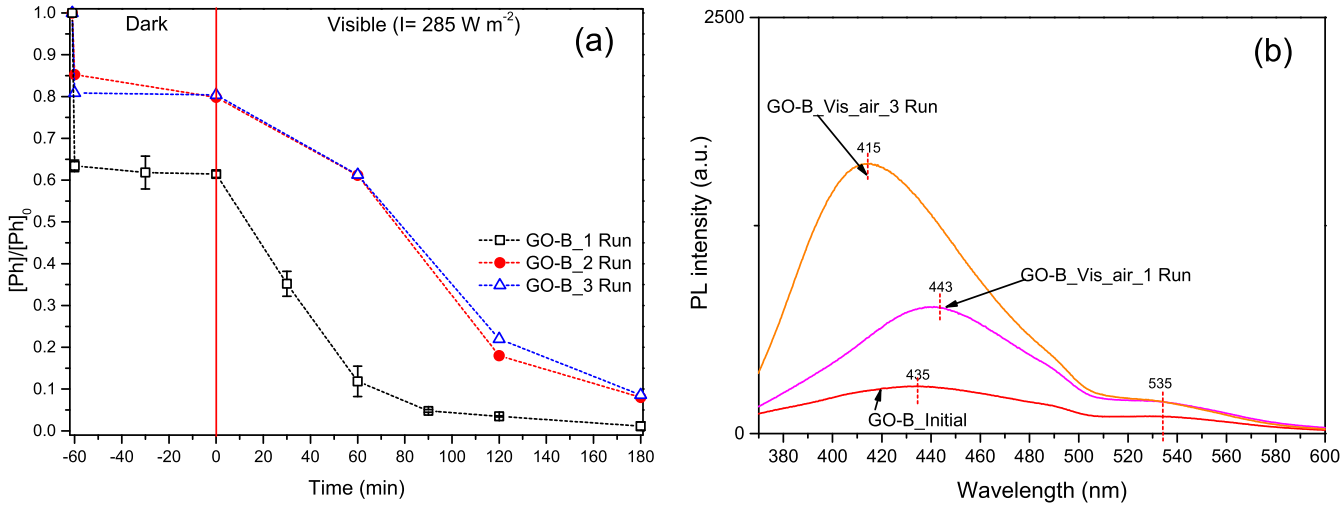

Fig. 10. (a) Reusability of GO-B under visible (Vis) illumination for the photocatalytic degradation of phenol (Ph). (b) PL measurements of the filtered phenol solution before and after photocatalysis with GO-B (excitation at 320 nm).

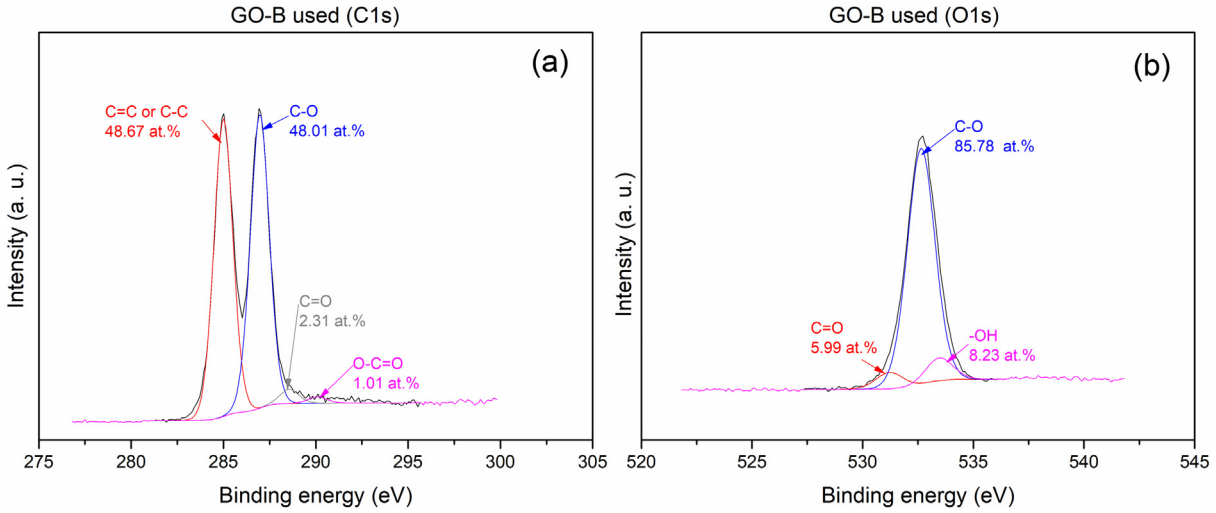

Fig. 11. XPS spectra for the deconvoluted (a) C1s and (b) O1s regions of GO-B used for three cycles of phenol degradation under visible illumination.

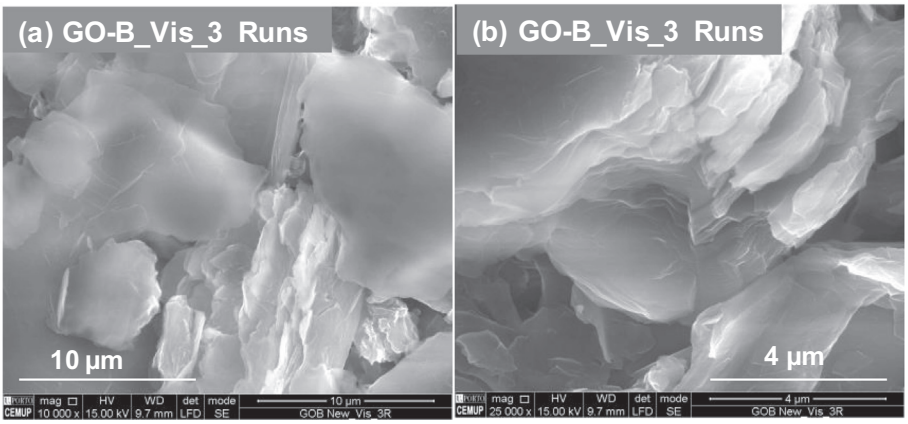

Fig. 12. SEM images of GO-B used for three cycles of phenol degradation under visible illumination.

To better understand this behaviour, pH measurements and PL spectra of the aqueous dispersions of GO-B and phenol were collected at the beginning (GO-B_Initial) and at the end of the 1st and 3rd cycles upon visible irradiation (Fig. 10b). The decrease/increase of pH was accompanied by a corresponding red/blue shift of the maximum emission wavelength, following the trends of other studies [62]. The pH values of the solutions irradiated with visible light showed a pH decrease from 4.9 (GO-B_Initial) to 4.5 after the 1st run and a pH increase to 5.4 after the 3rd run of irradiation. This system seemed to display reversibility regarding the pH variation in consecutive runs. The PL maximum emission wavelength of GO-B_Initial (435 nm) was red-shifted (higher wavelengths, 440 nm) after the 1st run (GO-B_Vis_1 Run), followed by another shift of this band to lower wavelengths close to the initial maximum emission wavelength (415 nm) after the 3rd run (GO-B_Vis_3 Run). The main contribution for this dependency of PL with pH can be ascribed to the presence of different oxygen functional groups in GO and their protonation and deprotonation [62].

Several studies in the literature reporting the reduction of GO with light exposure [27,28,78] prompted us to perform additional XPS analysis after three cycles of visible light irradiation (Fig. 11). A slight decrease in the oxygen content was observed from 25.80 at.% in the original GO-B to nearly 25.40 at.% after three consecutive runs. From the deconvolution of the C1s (Fig. 11a) and O1s spectra (Fig. 11b) of the material used for three cycles, no significant differences are observed with respect to the fresh GO-B (Fig. 3b and d, respectively), C—O slightly decreasing (from 53.83 to 48.01 at.% in C1s and from 87.57 to 85.78 at.% in O1s).

Furthermore, changes in the morphology of GO-B were not observed by SEM after three cycles of visible irradiation (Fig. 12) in comparison with the fresh material (Fig. 5c and d), corroborating the reusability of the photocatalyst.

4. Conclusions

Graphene oxide (GO) prepared by Brodie's method (GO-B) is a successful undoped metal-free photocatalyst for the degradation of phenol under near-UV/Vis and visible irradiation. GO-B presents a better performance than the most frequently reported GO analogue prepared by the modified Hummers' method (GO-H). Hence, the present study contributes to the still limited portfolio of undoped metal-free GO photocatalysts for the degradation of organic contaminants in aqueous media [30–35]. The lower amount of oxygen functionalities in GO-B *vs* GO-H (25.80 *vs* 34.60 at.%) and carbonyl groups in particular (1.29 *vs* 8.65 at.%, determined by XPS), the smaller interlayer distance (0.68 *vs* 0.74 nm calculated by XRD) and the lower photoluminescence intensity in liquid dispersion, respectively, explain the observed higher photocatalytic activity as a consequence of an efficient electron-hole charge separation. When in comparison with the literature [33,34], the GO-B potential for solar applications stands out, since it is a metal-free photocatalyst active under both UV and visible light. Moreover, this study opens new opportunities for further development of a GO-B based photocatalytic immobilized material for water treatment, more studies being needed for instance using real matrices.

CRediT authorship contribution statement

Marta Pedrosa: Methodology, Investigation, Data curation, Writing - original draft. **Eliana S. Da Silva:** Methodology, Writing - review & editing. **Luisa Pastrana-Martínez:** Methodology, Writing - review & editing. **Goran Drazic:** Investigation, Writing - review & editing. **Polycarpos Falaras:** Investigation, Writing - review & editing. **Joaquim L. Faria:** Methodology, Writing - review & editing. **José L. Figueiredo:** Supervision, Writing - review & editing. **Adrián M.T. Silva:** Conceptualization, Supervision, Funding acquisition, Writing - review & editing.

Declaration of Competing Interest

The authors declare that they have no known competing financial interests or personal relationships that could have appeared to influence the work reported in this paper.

Acknowledgements

This work was financially supported by project NORTE-01-0145-FEDER-031049 (InSpeCt) funded by FEDER funds through NORTE 2020 - Programa Operacional Regional do NORTE and by national funds (PIDDAC) through FCT/MCTES (PTDC/EAM-AMB/31049/2017). We would also like to thank the scientific collaboration under project "AIProcMat@N2020 - Advanced Industrial Processes and Materials for a Sustainable Northern Region of Portugal 2020" (NORTE-01-0145-FEDER-000006, NORTE 2020, Portugal 2020 Partnership Agreement, through FEDER), project "Associate Laboratory LSRE-LCM" (UID/EQU/50020/2019 - FCT/MCTES – PIDDAC) and project 2DMAT4FUEL (POCI-01-0145-FEDER-029600 - COMPETE2020 – FCT/MCTES - PIDDAC). MP acknowledges the PhD research grant from FCT (Ref. SFRH/BD/102086/2014). LMPM acknowledges the Spanish Ministry of Economy and Competitiveness (MINECO) and the European Social Fund for a Ramon y Cajal research contract (RYC-2016-19347). GD acknowledges the Slovenian Research Agency (P2-0393). PF

acknowledges support from Prince Sultan Bin Abdulaziz International Prize for Water–Alternative Water Resources Prize 2014. Technical assistance with SEM and XPS analysis is gratefully acknowledged to CEMUP team and Dr. Carlos Sá, and with XRD to Professor Pedro P.B. Tavares from Centro de Química–Vila Real, Universidade de Trás-os-Montes e Alto Douro.

Appendix A. Supplementary material

Supplementary data to this article can be found online at https://doi.org/10.1016/j.jcis.2020.01.093.

References

[1] K.-Q. Lu, L. Yuan, X. Xin, Y.-J. Xu, Hybridization of graphene oxide with commercial graphene for constructing 3D metal-free aerogel with enhanced photocatalysis, Appl. Catal. B 226 (2018) 16–22.
[2] C. Li, Y. Xu, W. Tu, G. Chen, R. Xu, Metal-free photocatalysts for various applications in energy conversion and environmental purification, Green Chem. 19 (2017) 882–899.
[3] S. Sajjad, S.A. Khan Leghari, A. Iqbal, Study of graphene oxide structural features for catalytic, antibacterial, gas sensing, and metals decontamination environmental applications, ACS Appl. Mater. Interfaces 9 (2017) 43393–43414.
[4] H.C. Hsu, I. Shown, H.Y. Wei, Y.C. Chang, H.Y. Du, Y.G. Lin, C.A. Tseng, C.H. Wang, L.C. Chen, Y.C. Lin, K.H. Chen, Graphene oxide as a promising photocatalyst for CO_2 to methanol conversion, Nanoscale 5 (2013) 262–268.
[5] S. Min, G. Lu, Dye-sensitized reduced graphene oxide photocatalysts for highly efficient visible-light-driven water reduction, J. Phys. Chem. C 115 (2011) 13938–13945.
[6] L.K. Putri, L.-L. Tan, W.-J. Ong, W.S. Chang, S.-P. Chai, Graphene oxide: exploiting its unique properties toward visible-light-driven photocatalysis, Appl. Mater. Today 4 (2016) 9–16.
[7] L.M. Pastrana-Martínez, S. Morales-Torres, A.G. Kontos, N.G. Moustakas, J.L. Faria, J.M. Doña-Rodríguez, P. Falaras, A.M.T. Silva, TiO_2, surface modified TiO_2 and graphene oxide-TiO_2 photocatalysts for degradation of water pollutants under near-UV/Vis and visible light, Chem. Eng. J. 224 (2013) 17–23.
[8] M. Pedrosa, L.M. Pastrana-Martínez, M.F.R. Pereira, J.L. Faria, J.L. Figueiredo, A. M.T. Silva, N/S-doped graphene derivatives and TiO_2 for catalytic ozonation and photocatalysis of water pollutants, Chem. Eng. J. 348 (2018) 888–897.
[9] T.-D. Nguyen-Phan, V.H. Pham, E.W. Shin, H.-D. Pham, S. Kim, J.S. Chung, E.J. Kim, S.H. Hur, The role of graphene oxide content on the adsorption-enhanced photocatalysis of titanium dioxide/graphene oxide composites, Chem. Eng. J. 170 (2011) 226–232.
[10] L.M. Pastrana-Martinez, S. Morales-Torres, V. Likodimos, J.L. Figueiredo, J.L. Faria, P. Falaras, A.M.T. Silva, Advanced nanostructured photocatalysts based on reduced graphene oxide-TiO_2 composites for degradation of diphenhydramine pharmaceutical and methyl orange dye, Appl. Catal. B 123 (2012) 241–256.
[11] L.K. Putri, W.J. Ong, W.S. Chang, S.P. Chai, Heteroatom doped graphene in photocatalysis: a review, Appl. Surf. Sci. 358 (2015) 2–14.
[12] B. Li, T. Liu, Y. Wang, Z. Wang, ZnO/graphene-oxide nanocomposite with remarkably enhanced visible-light-driven photocatalytic performance, J. Colloid Interface Sci. 377 (2012) 114–121.
[13] M. Xing, W. Fang, X. Yang, B. Tian, J. Zhang, Highly-dispersed boron-doped graphene nanoribbons with enhanced conductibility and photocatalysis, Chem. Commun. 50 (2014) 6637–6640.
[14] Z.R. Tang, Y. Zhang, N. Zhang, Y.J. Xu, New insight into the enhanced visible light photocatalytic activity over boron-doped reduced graphene oxide, Nanoscale 7 (2015) 7030–7034.
[15] W. Peng, X. Li, Synthesis of a sulfur-graphene composite as an enhanced metal-free photocatalyst, Nano Res. 6 (2013) 286–292.
[16] L.M. Pastrana-Martínez, S. Morales-Torres, V. Likodimos, P. Falaras, J.L. Figueiredo, J.L. Faria, A.M.T. Silva, Role of oxygen functionalities on the synthesis of photocatalytically active graphene–TiO_2 composites, Appl. Catal. B 158–159 (2014) 329–340.
[17] R. Bera, S. Kundu, A. Patra, 2D hybrid nanostructure of reduced graphene oxide–CdS nanosheet for enhanced photocatalysis, ACS Appl. Mater. Interfaces 7 (2015) 13251–13259.
[18] S. Linley, Y. Liu, C.J. Ptacek, D.W. Blowes, F.X. Gu, Recyclable graphene oxide-supported titanium dioxide photocatalysts with tunable properties, ACS Appl. Mater. Interfaces 6 (2014) 4658–4668.
[19] W. Zhang, Y. Li, S. Peng, Facile synthesis of graphene sponge from graphene oxide for efficient dye-sensitized H_2 evolution, ACS Appl. Mater. Interfaces 8 (2016) 15187–15195.
[20] Y. Deng, L. Tang, C. Feng, G. Zeng, J. Wang, Y. Lu, Y. Liu, J. Yu, S. Chen, Y. Zhou, Construction of plasmonic Ag and nitrogen-doped graphene quantum dots codecorated ultrathin graphitic carbon nitride nanosheet composites with enhanced photocatalytic activity: Full-spectrum response ability and mechanism insight, ACS Appl. Mater. Interfaces 9 (2017) 42816–42828.
[21] A.B. Bourlinos, V. Georgakilas, R. Zboril, T.A. Steriotis, A.K. Stubos, C. Trapalis, Aqueous-phase exfoliation of graphite in the presence of polyvinylpyrrolidone for the production of water-soluble graphenes, Solid State Commun. 149 (2009) 2172–2176.
[22] A.B. Bourlinos, V. Georgakilas, R. Zboril, T.A. Steriotis, A.K. Stubos, Liquid-phase exfoliation of graphite towards solubilized graphenes, Small 5 (2009) 1841–1845.
[23] A. Lerf, H. He, M. Forster, J. Klinowski, Structure of graphite oxide revisited, J. Phys. Chem. B 102 (1998) 4477–4482.
[24] T. Szabó, O. Berkesi, P. Forgó, K. Josepovits, Y. Sanakis, D. Petridis, I. Dékány, Evolution of surface functional groups in a series of progressively oxidized graphite oxides, Chem. Mater. 18 (2006) 2740–2749.
[25] K. Erickson, R. Erni, Z. Lee, N. Alem, W. Gannett, A. Zettl, Determination of the local chemical structure of graphene oxide and reduced graphene oxide, Adv. Mater. 22 (2010) 4467–4472.
[26] K.P. Loh, Q. Bao, G. Eda, M. Chhowalla, Graphene oxide as a chemically tunable platform for optical applications, Nat. Chem. 2 (2010) 1015–1024.
[27] M. Koinuma, C. Ogata, Y. Kamei, K. Hatakeyama, H. Tateishi, Y. Watanabe, T. Taniguchi, K. Gezuhara, S. Hayami, A. Funatsu, M. Sakata, Y. Kuwahara, S. Kurihara, Y. Matsumoto, Photochemical engineering of graphene oxide nanosheets, J. Phys. Chem. C 116 (2012) 19822–19827.
[28] W.C. Hou, I. Chowdhury, D.G. Goodwin Jr., W.M. Henderson, D.H. Fairbrother, D. Bouchard, R.G. Zepp, Photochemical transformation of graphene oxide in sunlight, Environ. Sci. Technol. 49 (2015) 3435–3443.
[29] J. Liu, J. Ke, D. Li, H. Sun, P. Liang, X. Duan, W. Tian, M.O. Tadé, S. Liu, S. Wang, Oxygen vacancies in shape controlled Cu_2O/reduced graphene oxide/In_2O_3 hybrid for promoted photocatalytic water oxidation and degradation of environmental pollutants, ACS Appl. Mater. Interfaces 9 (2017) 11678–11688.
[30] A.S. Adeleye, X. Wang, F. Wang, R. Hao, W. Song, Y. Li, Photoreactivity of graphene oxide in aqueous system: reactive oxygen species formation and bisphenol A degradation, Chemosphere 195 (2018) 344–350.
[31] J. Oh, Y.H. Chang, Y.H. Kim, S. Park, Thickness-dependent photocatalytic performance of graphite oxide for degrading organic pollutants under visible light, PCCP 18 (2016) 10882–10886.
[32] C. Li, Q. Xu, S. Xu, X. Zhang, X. Hou, P. Wu, Synergy of adsorption and photosensitization of graphene oxide for improved removal of organic pollutants, RSC Adv. 7 (2017) 16204–16209.
[33] K. Bustos-Ramirez, C.E. Barrera-Diaz, M. De Icaza, A.L. Martínez-Hernández, C. Velasco-Santos, Photocatalytic activity in phenol removal of water from graphite and graphene oxides: Effect of degassing and chemical oxidation in the synthesis process, J. Chem. 2015 (2015) 1–10.
[34] K. Bustos-Ramírez, C.E. Barrera-Díaz, M. De Icaza-Herrera, A.L. Martínez-Hernández, R. Natividad-Rangel, C. Velasco-Santos, 4-chlorophenol removal from water using graphite and graphene oxides as photocatalysts, J. Environ. Health Sci. Eng. 13 (2015) 33–43.
[35] E.E. Pérez-Ramírez, G. de la Rosa-Álvarez, P. Salas, C. Velasco-Santos, A.L. Martínez-Hernández, Comparison as effective photocatalyst or adsorbent of carbon materials of one, two, and three dimensions for the removal of reactive Red 2 in water, Environ. Eng. Sci. 32 (2015) 872–880.
[36] O. Jankovský, P. Marvan, M. Nováček, J. Luxa, V. Mazánek, K. Klímová, D. Sedmidubský, Z. Sofer, Synthesis procedure and type of graphite oxide strongly influence resulting graphene properties, Appl. Mater. Today 4 (2016) 45–53.
[37] C. Botas, P. Álvarez, P. Blanco, M. Granda, C. Blanco, R. Santamaría, L.J. Romasanta, R. Verdejo, M.A. López-Manchado, R. Menéndez, Graphene materials with different structures prepared from the same graphite by the Hummers and Brodie methods, Carbon 65 (2013) 156–164.
[38] H.L. Poh, F. Sanek, A. Ambrosi, G. Zhao, Z. Sofer, M. Pumera, Graphenes prepared by Staudenmaier, Hofmann and Hummers methods with consequent thermal exfoliation exhibit very different electrochemical properties, Nanoscale 4 (2012) 3515–3522.
[39] J.G. Moo, B. Khezri, R.D. Webster, M. Pumera, Graphene oxides prepared by Hummers', Hofmann's, and Staudenmaier's methods: dramatic influences on heavy-metal-ion adsorption, ChemPhysChem 15 (2014) 2922–2929.
[40] S. You, S.M. Luzan, T. Szabó, A.V. Talyzin, Effect of synthesis method on solvation and exfoliation of graphite oxide, Carbon 52 (2013) 171–180.
[41] A.V. Talyzin, G. Mercier, A. Klechikov, M. Hedenström, D. Johnels, D. Wei, D. Cotton, A. Opitz, E. Moons, Brodie vs Hummers graphite oxides for preparation of multi-layered materials, Carbon 115 (2017) 430–440.
[42] C.K. Chua, Z. Sofer, M. Pumera, Graphite oxides: effects of permanganate and chlorate oxidants on the oxygen composition, Chem. – A Eur. J. 18 (2012) 13453–13459.
[43] B.C. Brodie, Sur le poids atomique du graphite, Annales de Chimie et de Physique 59 (1860) 466–472.
[44] W.S. Hummers, R.E. Offeman, Preparation of graphitic oxide, J. Am. Chem. Soc. 80 (1958). 1339 1339.
[45] L.M. Pastrana-Martinez, S. Morales-Torres, J.L. Figueiredo, J.L. Faria, A.M.T. Silva, Graphene oxide based ultrafiltration membranes for photocatalytic degradation of organic pollutants in salty water, Water Res. 77 (2015) 179–190.
[46] J. Rivera-Utrilla, I. Bautista-Toledo, M.A. Ferro-García, C. Moreno-Castilla, Activated carbon surface modifications by adsorption of bacteria and their effect on aqueous lead adsorption, J. Chem. Technol. Biotechnol. 76 (2001) 1209–1215.
[47] M.P. Araújo, O.S.G.P. Soares, A.J.S. Fernandes, M.F.R. Pereira, C. Freire, Tuning the surface chemistry of graphene flakes: new strategies for selective oxidation, RSC Adv. 7 (2017) 14290–14301.

[48] D.R. Dreyer, A.D. Todd, C.W. Bielawski, Harnessing the chemistry of graphene oxide, Chem. Soc. Rev. 43 (2014) 5288–5301.
[49] A. Ganguly, S. Sharma, P. Papakonstantinou, J. Hamilton, Probing the thermal deoxygenation of graphene oxide using high-resolution In Situ X-ray-based spectroscopies, J. Phys. Chem. C 115 (2011) 17009–17019.
[50] C.-M. Chen, J.-Q. Huang, Q. Zhang, W.-Z. Gong, Q.-H. Yang, M.-Z. Wang, Y.-G. Yang, Annealing a graphene oxide film to produce a free standing high conductive graphene film, Carbon 50 (2012) 659–667.
[51] L.K. Putri, B.-J. Ng, K.H. Tan, F.S. Lim, W.-J. Ong, W.S. Chang, S.-P. Chai, Tailoring the properties of oxygenated graphene with different oxidation degrees for noble-metal-free photocatalytic hydrogen evolution, Catal. Today 315 (2018) 93–102.
[52] A. Esteban-Arranz, D. Compte-Tordesillas, V. Muñoz-Andrés, M. Pérez-Cadenas, A. Guerrero-Ruiz, Effect of surface, structural and textural properties of graphenic materials over cooperative and synergetic adsorptions of two chloroaromatic compounds from aqueous solution, Catal. Today 301 (2018) 104–111.
[53] M. Seredych, T.J. Bandosz, Mechanism of ammonia retention on graphite oxides: role of surface chemistry and structure, J. Phys. Chem. C 111 (2007) 15596–15604.
[54] M. Seredych, C. Petit, A.V. Tamashausky, T.J. Bandosz, Role of graphite precursor in the performance of graphite oxides as ammonia adsorbents, Carbon 47 (2009) 445–456.
[55] M. Sabzevari, D.E. Cree, L.D. Wilson, Gas and solution uptake properties of graphene oxide-based composite materials: organic vs. inorganic cross-linkers, Journal of Composites, Science 3 (2019) 80.
[56] B. Lian, S. De Luca, Y. You, S. Alwarappan, M. Yoshimura, V. Sahajwalla, S.C. Smith, G. Leslie, R.K. Joshi, Extraordinary water adsorption characteristics of graphene oxide, Chem. Sci. 9 (2018) 5106–5111.
[57] M. Seredych, A.V. Tamashausky, T.J. Bandosz, Graphite oxides obtained from porous graphite: The role of surface chemistry and texture in ammonia retention at ambient conditions, Adv. Funct. Mater. 20 (2010) 1670–1679.
[58] W. Xie, L.T. Weng, C.K. Chan, K.L. Yeung, C.M. Chan, Reactions of SO_2 and NH_3 with epoxy groups on the surface of graphite oxide powder, Phys Chem Chem Phys 20 (2018) 6431–6439.
[59] C. Petit, M. Seredych, T.J. Bandosz, Revisiting the chemistry of graphite oxides and its effect on ammonia adsorption, J. Mater. Chem. 19 (2009) 9176–9185.
[60] Y. Bian, Z.-Y. Bian, J.-X. Zhang, A.-Z. Ding, S.-L. Liu, H. Wang, Effect of the oxygen-containing functional group of graphene oxide on the aqueous cadmium ions removal, Appl. Surf. Sci. 329 (2015) 269–275.
[61] M. Pedrosa, G. Drazic, P.B. Tavares, J.L. Figueiredo, A.M.T. Silva, Metal-free graphene-based catalytic membrane for degradation of organic contaminants by persulfate activation, Chem. Eng. J. 369 (2019) 223–232.
[62] P. Dutta, D. Nandi, S. Datta, S. Chakraborty, N. Das, S. Chatterjee, U.C. Ghosh, A. Halder, Excitation wavelength dependent UV fluorescence of dispersed modified graphene oxide: effect of pH, J. Lumin. 168 (2015) 269–275.
[63] T. Olmez-Hanci, I. Arslan-Alaton, S. Gurmen, I. Gafarli, S. Khoei, S. Safaltin, D. Yesiltepe Ozcelik, Oxidative degradation of Bisphenol A by carbocatalytic activation of persulfate and peroxymonosulfate with reduced graphene oxide, J. Hazard. Mater. 360 (2018) 141–149.
[64] L. Stobinski, B. Lesiak, A. Malolepszy, M. Mazurkiewicz, B. Mierzwa, J. Zemek, P. Jiricek, I. Bieloshapka, Graphene oxide and reduced graphene oxide studied by the XRD, TEM and electron spectroscopy methods, J. Electron Spectrosc. Relat. Phenom. 195 (2014) 145–154.
[65] A. Tararan, A. Zobelli, A.M. Benito, W.K. Maser, O. Stéphan, Revisiting graphene oxide chemistry via spatially-resolved electron energy loss spectroscopy, Chem. Mater. 28 (2016) 3741–3748.
[66] H. Yan, H. Wu, K. Li, Y. Wang, X. Tao, H. Yang, A. Li, R. Cheng, Influence of the surface structure of graphene oxide on the adsorption of aromatic organic compounds from water, ACS Appl Mater Interfaces 7 (2015) 6690–6697.
[67] Z. Pei, L. Li, L. Sun, S. Zhang, X.-Q. Shan, S. Yang, B. Wen, Adsorption characteristics of 1,2,4-trichlorobenzene, 2,4,6-trichlorophenol, 2-naphthol and naphthalene on graphene and graphene oxide, Carbon 51 (2013) 156–163.
[68] M. Aleksandrzak, W. Kukulka, E. Mijowska, Graphitic carbon nitride/graphene oxide/reduced graphene oxide nanocomposites for photoluminescence and photocatalysis, Appl. Surf. Sci. 398 (2017) 56–62.
[69] G. Eda, Y.Y. Lin, C. Mattevi, H. Yamaguchi, H.A. Chen, I.S. Chen, C.W. Chen, M. Chhowalla, Blue photoluminescence from chemically derived graphene oxide, Adv. Mater. 22 (2010) 505–509.
[70] J. Shang, L. Ma, J. Li, W. Ai, T. Yu, G.G. Gurzadyan, The origin of fluorescence from graphene oxide, Sci. Rep. 2 (2012) 792–799.
[71] D. Du, H. Song, Y. Nie, X. Sun, L. Chen, J. Ouyang, Photoluminescence of graphene oxide in visible range arising from excimer formation, J. Phys. Chem. C 119 (2015) 20085–20090.
[72] C.T. Chien, S.S. Li, W.J. Lai, Y.C. Yeh, H.A. Chen, I.S. Chen, L.C. Chen, K.H. Chen, T. Nemoto, S. Isoda, M. Chen, T. Fujita, G. Eda, H. Yamaguchi, M. Chhowalla, C.W. Chen, Tunable photoluminescence from graphene oxide, Angew. Chem. Int. Ed. 51 (2012) 6662–6666.
[73] O.N. Tchaikovskaya, I.V. Sokolova, R.T. Kuznetsova, V.A. Swetlitchnyi, T.N. Kopylova, G.V. Mayer, Fluorescence investigations of phenol phototransformation in aqueous solutions, J. Fluoresc. 10 (2000) 403–408.
[74] Z. Wang, W. Cai, X. Hong, X. Zhao, F. Xu, C. Cai, Photocatalytic degradation of phenol in aqueous nitrogen-doped TiO_2 suspensions with various light sources, Appl. Catal. B 57 (2005) 223–231.
[75] M.Q. Yang, Y. Zhang, N. Zhang, Z.R. Tang, Y.J. Xu, Visible-light-driven oxidation of primary C-H bonds over CdS with dual co-catalysts graphene and TiO_2, Sci. Rep. 3 (2013) 3314–3321.
[76] R. Palominos, J. Freer, M.A. Mondaca, H.D. Mansilla, Evidence for hole participation during the photocatalytic oxidation of the antibiotic flumequine, J. Photochem. Photobiol. A 193 (2008) 139–145.
[77] A. Gómez-Avilés, M. Peñas-Garzón, J. Bedia, J.J. Rodriguez, C. Belver, C-modified TiO_2 using lignin as carbon precursor for the solar photocatalytic degradation of acetaminophen, Chem. Eng. J. 358 (2019) 1574–1582.
[78] Y.-L. Zhang, L. Guo, H. Xia, Q.-D. Chen, J. Feng, H.-B. Sun, Photoreduction of graphene oxides: methods, properties, and applications, Adv. Opt. Mater. 2 (2014) 10–28.